State-dependent barium block of wild-type and inactivation-deficient HERG channels in *Xenopus* oocytes

Manjula Weerapura*†, Stanley Nattel*†‡, Marc Courtemanche*§, David Doern*, Nathalie Ethier* and Terence E. Hébert*‖

*Research Center, Departments of ‡Medicine and ‖Anesthesia, Montreal Heart Institute, 5000 Belanger Street East, Montreal, Departments of ‡Medicine, ‖Anesthesia and Biochemistry and §Physiology, University of Montreal, PO Box 6128, Succursale Centre-ville, Montreal and †Department of Pharmacology and Therapeutics, McGill University, 3655 Promenade Sir-William-Osler, Montreal, Quebec, Canada

(Received 4 January 2000; accepted after revision 25 April 2000)

1. The effects of Ba^{2+} on current resulting from the heterologous expression of the human *ether-à-go-go* related gene (*HERG*) (I_{HERG}) was studied with two-electrode voltage clamp techniques in *Xenopus* oocytes.

2. Ba^{2+} produced time- and voltage-dependent block of I_{HERG}. Significant inhibition was seen at concentrations as low as 1 μM. Inhibition was greatest at step potentials between −40 and 0 mV; at more positive potentials, inhibition decreased in association with time-dependent unblocking of channels.

3. An inactivation-attenuated mutant of HERG (S631A) was prepared and expressed in *Xenopus* oocytes. Ba^{2+} block of S631A differed from that of HERG in that extensive unblocking was no longer seen at positive potentials and the voltage dependence of step current block was greatly attenuated.

4. A mathematical model was applied to analyse quantitatively the inhibitory effects of Ba^{2+} on I_{HERG}. The model suggested similar voltage-dependent affinity of Ba^{2+} for the open and closed states, along with absence of binding to the inactivated state, and accounted well for Ba^{2+} effects on both wild-type and S631A channels.

5. We conclude that Ba^{2+} potently inhibits I_{HERG} in a characteristic state-dependent fashion, with strong unblocking at positive potentials related to the presence of an intact C-type inactivation mechanism.

The delayed rectifier potassium current (I_K) is a key cardiac repolarizing current in a large number of species and tissues (Giles & Shibata, 1985; Colatsky *et al.* 1990; Balser *et al.* 1990; Anumonwo *et al.* 1992; Barry & Nerbonne, 1996). It consists of at least two components, the rapidly activating component, I_{Kr} and the slowly activating component, I_{Ks} (Noble & Tsien, 1969; Sanguinetti & Jurkiewicz, 1990, 1991).

Our understanding of the properties of I_K has been greatly advanced by the identification of important molecular components of both I_{Kr} and I_{Ks}. The products of *HERG* (Sanguinetti *et al.* 1995; Trudeau *et al.* 1995) and *KvLQT1* (Barhanin *et al.* 1996; Sanguinetti *et al.* 1996) represent the pore-forming subunits of I_{Kr} and I_{Ks}, respectively. The products of the *MiRP1* (Abbott *et al.* 1999) and *minK* (Barhanin *et al.* 1996; Sanguinetti *et al.* 1996) genes co-assemble with HERG and KvLQT1 *in vivo* to form I_{Kr} and I_{Ks} channels, respectively. Mutations at *HERG* or *KvLQT1* loci are associated with the long QT syndrome, an inherited form of potentially lethal heart disease (Curran *et al.* 1995; Wang *et al.* 1996). Recently, double mutations at these loci have been identified in some patients severely affected by the long QT syndrome (Berthet *et al.* 1999). Due to the clinical importance of these syndromes, substantial effort continues to be dedicated to the detailed study of the characteristics of HERG and KvLQT1, especially with regard to pore structure and block by various compounds and metal ions.

Cations are widely used to probe the structure of K^+ channels because of the ease with which they are able to access deeper pore regions, which may not be accessible by more sterically bulky drugs or toxins. One of the cations that is of special interest is Ba^{2+}, which has a similar crystal radius to K^+ (0·270 nm for Ba^{2+} *vs.* 0·266 nm for K^+) but is largely impermeable in K^+ channel pores. Larger cations such as Tl^+ (0·295 nm), Rb^+ (0·295 nm) and NH_4^+ (0·286 nm) exhibit significant pore permeation (see Hille, 1992, for a review), and the non-permeation of Ba^{2+} is

probably due to its divalent charge which results in a tight association with one or more K^+ interaction sites in the open pore. Ba^{2+} interacts strongly with a variety of K^+ channels from the intracellular or the extracellular sides of the membrane (Eaton & Brodwick, 1980; Armstrong *et al.* 1982; Miller *et al.* 1987; Taglialatela *et al.* 1993; Zang *et al.* 1995; Hurst *et al.* 1995). Ba^{2+} block is generally voltage dependent, reflecting the effect of the transmembrane voltage field on Ba^{2+} access to its binding site within the channel. Ba^{2+} effects on currents carried by HERG expressed in *Xenopus* oocytes have been reported to be either time and voltage independent (Trudeau *et al.* 1995) or voltage dependent (Ho *et al.* 1999). A better understanding of the Ba^{2+}–HERG interaction could provide insight into biophysical properties of the channel. We therefore conducted the present study to determine in detail how Ba^{2+} affects I_{HERG}. Because Ba^{2+} effects showed strong voltage and time dependence, we used a mathematical model to test quantitatively a conceptual model of state-dependent Ba^{2+} interactions with the HERG channel. Results of the present study have been previously presented in abstract form (Weerapura *et al.* 1998).

METHODS

Oocyte isolation and cRNA injection

Female *Xenopus laevis* were anaesthetized in 0·13% w/v tricaine for 30 min at 4 °C. Segments of the ovarian lobe were removed through a small abdominal incision. Up to four collections were made from each frog with adequate time allowed for healing between each. After the final collection frogs were killed by exsanguination following a lethal overdose of anaesthetic. The follicular layer was removed by digestion for 1 h with 6 units ml^{-1} collagenase (Sigma) in Ca^{2+}-free Barth's solution (NaCl, 88 mM; KCl, 1 mM; $NaHCO_3$, 2·4 mM; $MgSO_4$, 0·82 mM; Hepes, 5 mM; pH 7·6; supplemented with 10 mg ml^{-1} penicillin–streptomycin). The oocytes were incubated at 17 °C in L-15 media (50% v/v Leibowitz's L-15 media, 0·4-g l^{-1} glutamine, 8 mM Hepes, 40 mg l^{-1} gentamicin, pH 7·6). For *in vitro* transcription, *HERG* cDNA subcloned into pSP64 plasmid vector was linearized with *Eco*R1 (New England Bio Labs) and then transcribed with SP6 RNA polymerase (Ambion) for 1·5–2 h at 37 °C. Twenty four hours after the isolation procedure, stage IV and V oocytes were injected with 25–50 nl of *HERG* cRNA (~20–40 ng $oocyte^{-1}$).

Electrophysiology

Currents were recorded with the two-electrode voltage clamp technique from oocytes 1–3 days after injection of cRNA. Voltage commands were delivered via the GeneClamp 500 amplifier with

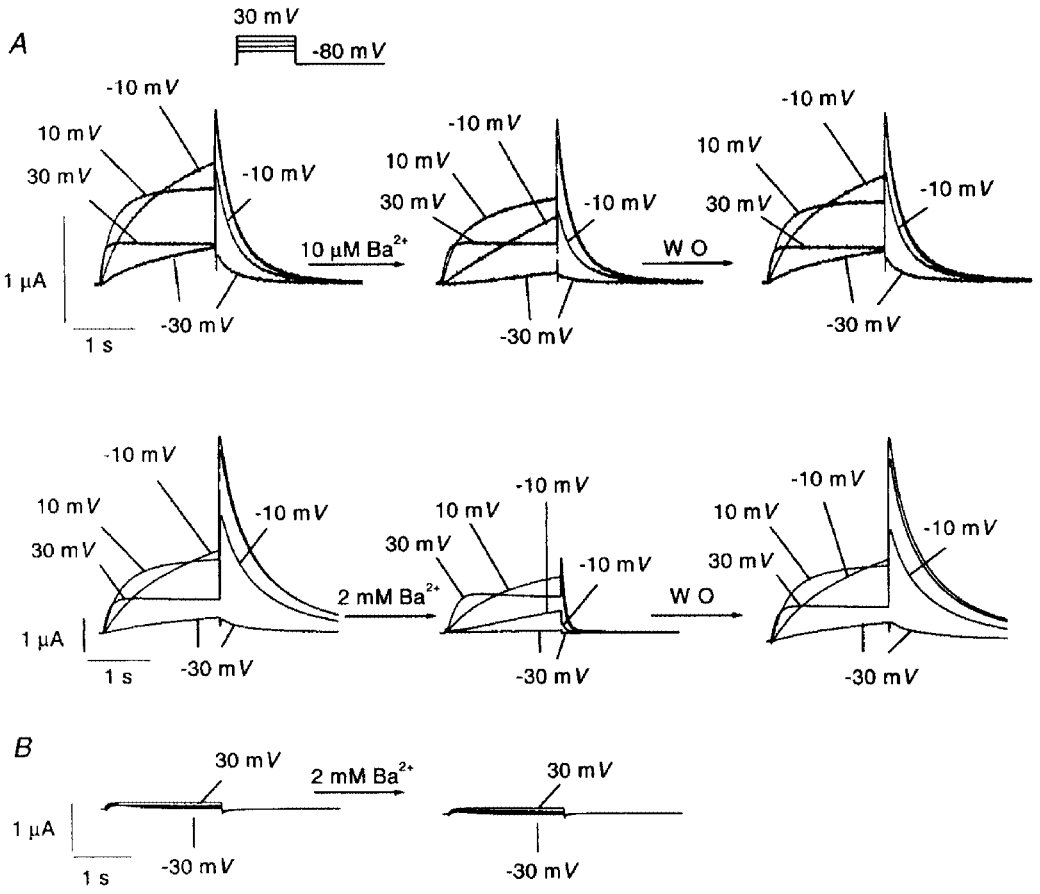

Figure 1. Concentration-dependent effects of Ba^{2+} on I_{HERG}

A, original recordings showing effects of 10 μM and 2 mM Ba^{2+} on I_{HERG} in one oocyte each. I_{HERG} was recorded with 2 s pulses to the voltages indicated (protocol inset). Leftmost panels are control recordings. Inhibitory effects were recorded 3 min after Ba^{2+}superfusion (centre panels). Effects were reversible upon 12 min of washout (WO, right panels). Capacitance transients have been blanked out. *B*, typical example of currents recorded from water-injected oocytes before (left) and after (right) exposure to 2 mM Ba^{2+}.

the use of pCLAMP 6 software (Axon Instruments). Currents were recorded at room temperature in ND96 (ionic components (mM): NaCl, 96; KCl, 2; $CaCl_2$, 1·8; $MgCl_2$, 1; Hepes, 5; pH 7·5). Solutions containing Ba^{2+} were prepared by adding appropriate volumes of a 0·2 M stock prepared in distilled water. All voltage clamp protocols in the presence of Ba^{2+} were applied after 3 min of perfusion with Ba^{2+} at a given concentration to ensure steady state conditions. To examine the possibility of surface charge screening effects of Ba^{2+}, we tested Ba^{2+} effects on oocytes treated with neuraminidase (Type X from *Clostridium perfringens*, Sigma). Endogenous currents from oocytes ($n = 6$) were recorded in the absence and presence of 2 mM Ba^{2+} 2 days after water injection.

Glass microelectrodes (borosilicate with filament) were pulled using a Flaming/Brown micropipette puller (Sutter Instruments). Pipettes had resistances of 1–3 MΩ for the voltage-sensing electrode and 0·1–0·5 MΩ for the current-injecting electrode when filled with 3 M KCl. The tips of the current-injecting electrodes were back-filled with 1% agarose in 3 M KCl to prevent KCl leakage (Hebert *et al.* 1994). ClampFit (Axon) and Origin (version 4, Microcal Software) were used for curve fitting. Data are presented as the means ± S.E.M. Statistical comparisons were made with Student's paired t test.

RESULTS

Ba^{2+} block of wild-type I_{HERG}

Figure 1*A* (left panels) shows I_{HERG} upon 2 s depolarizations from a holding potential (V_h) of −80 mV (12 s interpulse interval) 2 days after *HERG* cRNA injection. Note the increase in time-dependent outward current amplitudes at the lower voltages (−30 and −10 mV) and a subsequent reduction at more positive potentials due to intrinsic voltage-dependent fast C-type inactivation. In contrast, tail currents recorded upon returning to −80 mV increased in amplitude with stronger depolarizing pulses because of rapid recovery from inactivation at the V_h. The middle panels of Fig. 1*A* illustrate the effects of 10 μM and 2 mM

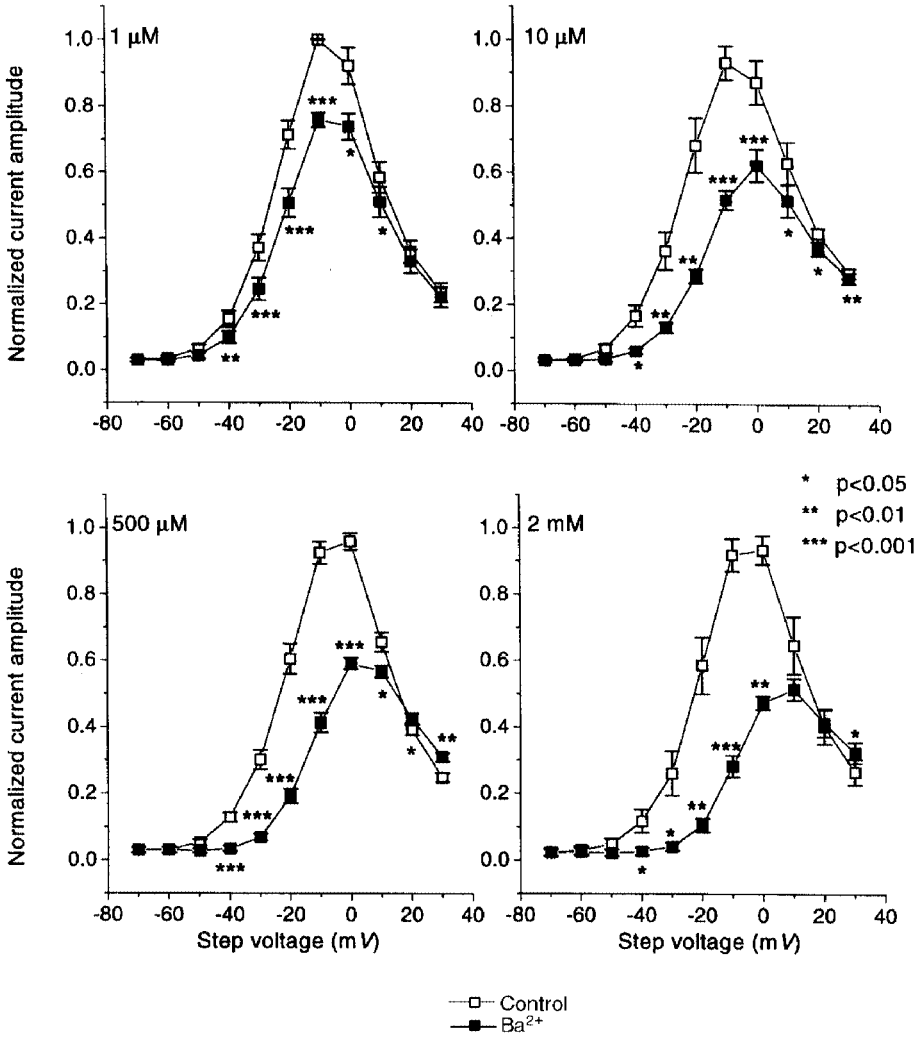

Figure 2. Mean data for Ba^{2+} inhibition of HERG step current

Step current amplitudes at the end of the 2 s pulses were measured before and after 3 min of perfusion with the indicated Ba^{2+} concentrations. Currents in each oocyte were normalized to the maximum current under control conditions, to control for varying current amplitudes among oocytes. The results shown are from 5, 5, 5 and 4 oocytes at 1, 10, 500 μM and 2 mM Ba^{2+}, respectively. Data are plotted as means ± S.E.M.; $*P < 0·05$, $**P < 0·01$, $***P < 0·001$ *vs.* control).

Ba^{2+}. With 10 μM Ba^{2+}, inhibition of step and tail current is evident at voltages of −30 and −10 mV, without apparent effects on currents at more positive potentials nor on tail current kinetics. At a 2 mM concentration, Ba^{2+} blocked step current at intermediate voltages, whereas at the most positive step potential tested (+30 mV), Ba^{2+} had little inhibitory effect on step current but inhibited the tail current. In addition to reducing maximum tail current amplitude, 2 mM Ba^{2+} also accelerated tail current decay. The inhibitory effects of Ba^{2+} were reversible upon washout (Fig. 1*A*, right panels). In order to evaluate the potential contaminating role of endogenous currents, currents were recorded from six water-injected oocytes with the same voltage protocol before and after 2 mM Ba^{2+}. As shown in Fig. 1*B* (left), the endogenous conductance was much smaller than I_{HERG}, with a maximum endogenous step current at +30 mV averaging $< 8\%$ of the I_{HERG} step current at the same voltage. Ba^{2+} had no effect on endogenous currents (Fig. 1*B*, right).

Mean data for Ba^{2+} effects on step currents at the end of 2 s test pulses are shown in Fig. 2. Data are normalized to the maximum step current in each oocyte to control for inter-oocyte variation in current amplitude. Significant inhibition was seen at all voltages between −40 and 0 mV for all concentrations tested. Ba^{2+} block decreased substantially at voltages on the descending limb of the I_{HERG} current–voltage relation (i.e. > 0 mV), corresponding to voltages with increasingly important inactivation.

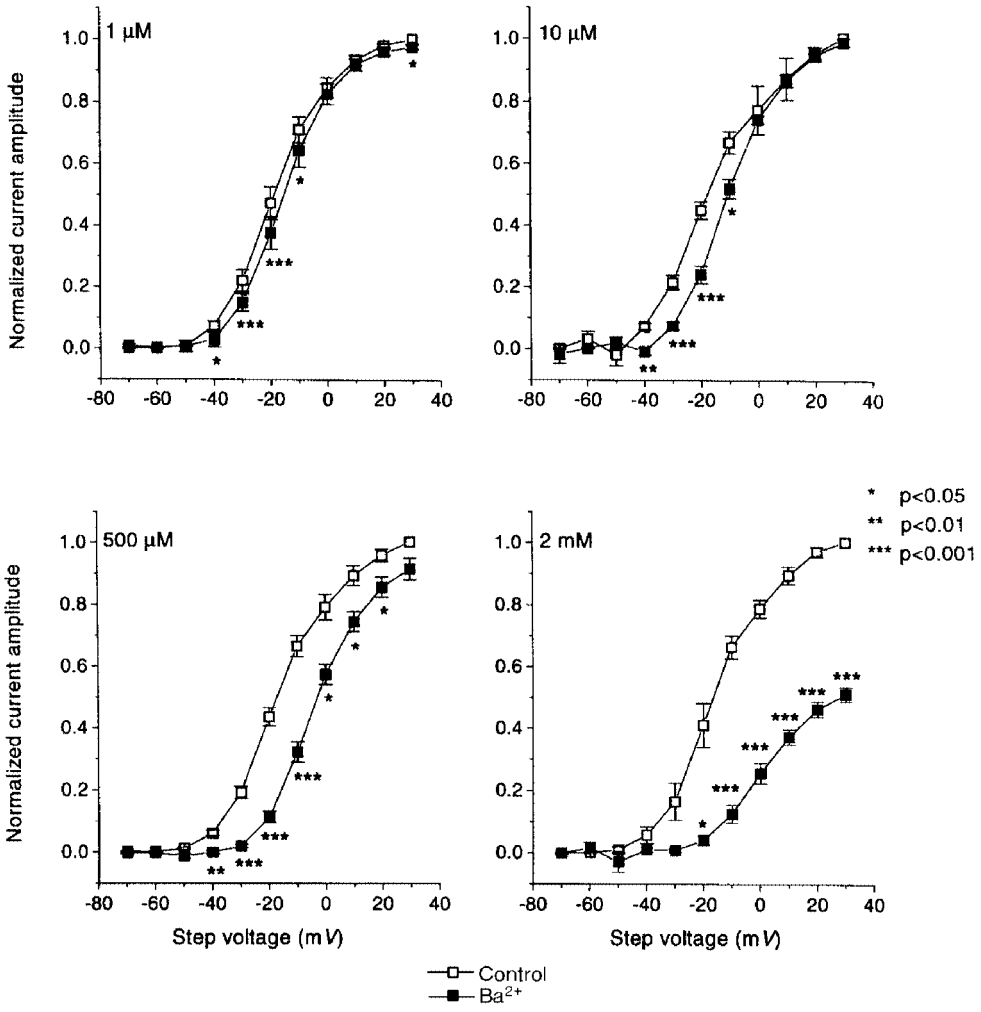

Figure 3. Inhibition of HERG tail current by various concentrations of Ba^{2+}

Results are means ± S.E.M. for 5, 5, 5 and 4 oocytes studied before and after 1, 10, 500 μM and 2 mM Ba^{2+}, respectively. Tail currents were recorded returning to the V_h of −80 mV following 2 s steps to the voltages indicated. Current amplitudes were estimated by fitting the deactivation phase of the tails to biexponential functions and extrapolating back to the beginning of the repolarizing step. All currents were normalised to the maximum control current amplitude (*$P < 0{\cdot}05$, **$P < 0{\cdot}01$, ***$P < 0{\cdot}001$ *vs.* control). Data were fitted to Boltzman functions ($I_{HERG} = (1 + \exp[(V_{½} + V_t/k)])^{-1}$) where $V_{½}$ is the half-activation voltage, V_t is the test voltage applied and k is the slope factor. $V_{½}$ and k (in mV) estimated from the fits were: $-18{\cdot}9 \pm 0{\cdot}5$, $9{\cdot}7 \pm 0{\cdot}5$; $-17{\cdot}7 \pm 1$, $11{\cdot}1 \pm 1{\cdot}0$; $-17{\cdot}2 \pm 0{\cdot}7$, $10{\cdot}5 \pm 0{\cdot}7$; $-16{\cdot}3 \pm 0{\cdot}7$, $10{\cdot}1 \pm 0{\cdot}7$ under control conditions and $-16{\cdot}0 \pm 0{\cdot}5$, $8{\cdot}7 \pm 0{\cdot}4$; $-10{\cdot}7 \pm 1$, $9{\cdot}0 \pm 1{\cdot}0$; $-4{\cdot}4 \pm 0{\cdot}8$, $8{\cdot}9 \pm 0{\cdot}7$; $1{\cdot}0 \pm 1{\cdot}7$, $9{\cdot}6 \pm 1{\cdot}4$ mV for 1, 10, 500 μM and 2 mM Ba^{2+}, respectively.

Mean data for Ba^{2+} effects on peak tail current amplitude are shown in Fig. 3. A concentration-dependent inhibition of tail current was observed, with minimal effects at 1 μM, inhibition at voltages between −40 and −10 mV noted at 10 μM and inhibition at all potentials positive to −40 mV with 500 μM and 2 mM Ba^{2+}. The half-maximal activation voltages ($V_{½}$) were estimated by Boltzmann fits to tail current data. $V_{½}$ averaged $-18{\cdot}9 \pm 0{\cdot}5$, $-17{\cdot}7 \pm 1$, $-17{\cdot}2 \pm 0{\cdot}7$ and $-16{\cdot}3 \pm 0{\cdot}7$ mV under control conditions and $-16 \pm 0{\cdot}5$, $-10{\cdot}7 \pm 1$, $-4{\cdot}4 \pm 0{\cdot}8$ and $1{\cdot}0 \pm 1{\cdot}7$ mV after 1 μM, 10 μM, 500 μM and 2 mM Ba^{2+}, respectively.

The reversal of Ba^{2+}-induced I_{HERG} inhibition at positive voltages (Fig. 2) was further studied by analysing the evolution of block over time during depolarizing pulses. Figure 4 shows original recordings of I_{HERG} before and after exposure to 500 μM Ba^{2+} at 0 and 30 mV (top panel), along with quantitative plots of Ba^{2+}-induced block in the same experiment during 2 s pulses to each of the six voltages indicated (lower panel). Fractional block is maximal towards the beginning of the pulse, and decreases thereafter at a rate that is voltage dependent. Unblocking is slowest at the most negative voltages and becomes increasingly rapid and more complete at positive potentials associated with prominent fast inactivation. Thus Ba^{2+} appears to unblock from HERG channels upon depolarization to positive voltages. Block is re-established upon repolarization to −80 mV, as indicated by the acceleration of tail current deactivation (Fig. 1). Tail current block is established at a rate that becomes increasingly rapid as Ba^{2+} concentration increases; e.g. $\tau = 207 \pm 19$ and 71 ± 10 ms for 100 μM ($n = 6$) and 2 mM Ba^{2+} ($n = 4$), respectively.

Ba^{2+} block of the inactivation-deficient mutant S631A

Ba^{2+} unblocking at voltages at which inward rectification due to rapid inactivation becomes prominent, and re-blocking at more negative voltages at which inactivation is removed, suggest that *HERG* inactivation interferes with Ba^{2+} block. To evaluate further the potential role of rapid inactivation in governing the effects of Ba^{2+} on I_{HERG}, we created the inactivation-attenuated mutant S631A (Zou *et al.* 1998). The single amino acid substitution in the mutant

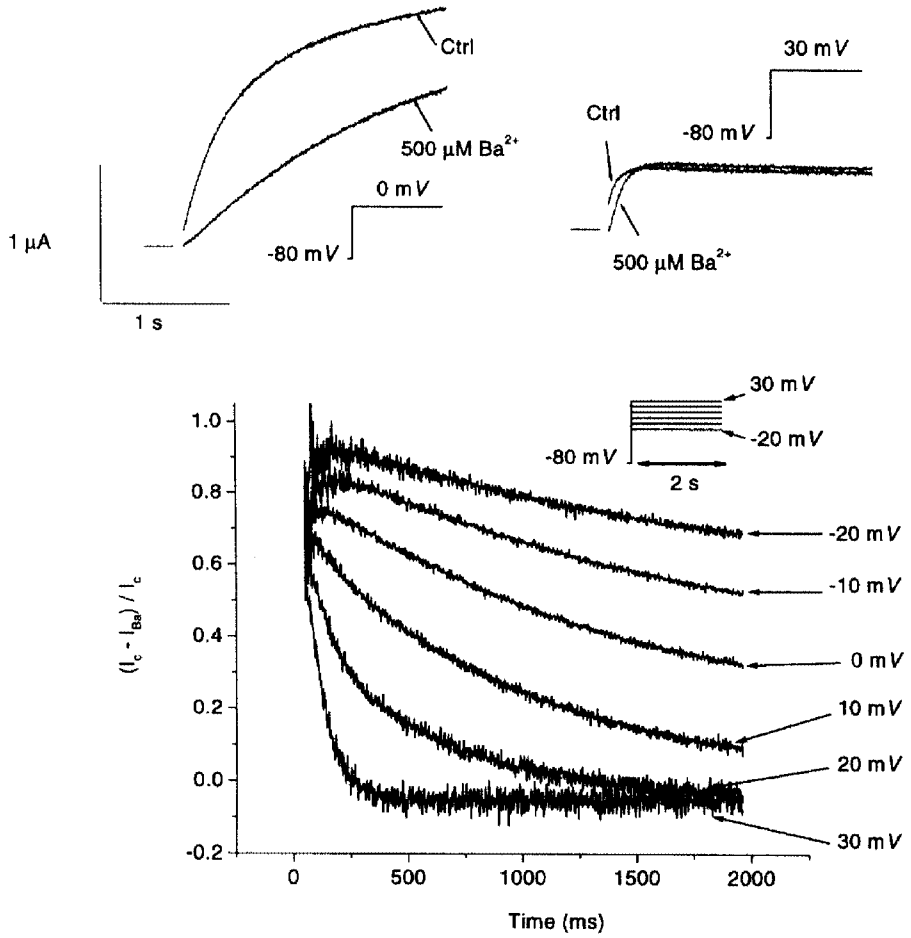

Figure 4. Evolution of Ba^{2+} block of I_{HERG} during depolarization

Top, original recordings during 2 s depolarizations to 0 mV (left) and 30 mV (right) before and after superfusion with 500 μM Ba^{2+}. Capacitive transients have been removed. Horizontal bars indicate zero current levels for the adjacent traces. Bottom, evolution of fractional block $(I_c - I_{Ba})/I_c$, where I_c and I_{Ba} are currents under control conditions and in the presence of 500 μM Ba^{2+}, respectively, in the same experiment, upon depolarization to the 6 voltage levels indicated. Similar results were obtained in 4 other oocytes.

is sufficient to shift the voltage dependence of inactivation by about 100 mV in the depolarizing direction. Thus, within the voltage range used in these studies, the channels are inactivation deficient and show greatly reduced inward rectification (Fig. 5*A*, left panels) compared with the wild-type (Fig. 1). The effect of Ba^{2+} was markedly altered in the S631A mutant. The qualitatively different behaviour of Ba^{2+} block at different test potentials noted for wild-type I_{HERG} (Figs 1 and 2) was replaced by qualitatively similar responses at each test potential in the mutant (Fig. 5*A*). Figure 5*B* shows mean (± S.E.M.) I_{S631A} step current under control conditions and in the presence of 1, 10, 500 μM and 2 mM Ba^{2+} ($n = 5$, 5, 5 and 7 oocytes, respectively). Significant reductions in current were produced at all voltages positive to −40 mV by Ba^{2+} concentrations of 10 μM or greater.

Figure 6 illustrates the evolution of block of I_{S631A} by 500 μM Ba^{2+} (compare with Fig. 4). At 0 mV, the response to Ba^{2+} is qualitatively comparable to that of wild-type channels; however, at 30 mV there is a major difference. The strong time-dependent unblocking noted in wild-type channels is lost. The differences between wild-type and mutant channels are further illustrated by the plot of block as a function of time at step voltages between −20 and +30 mV (Fig. 6, lower panel). In place of the important unblocking at positive voltages observed for the wild-type (Fig. 4) only a modest degree of unblocking occurs.

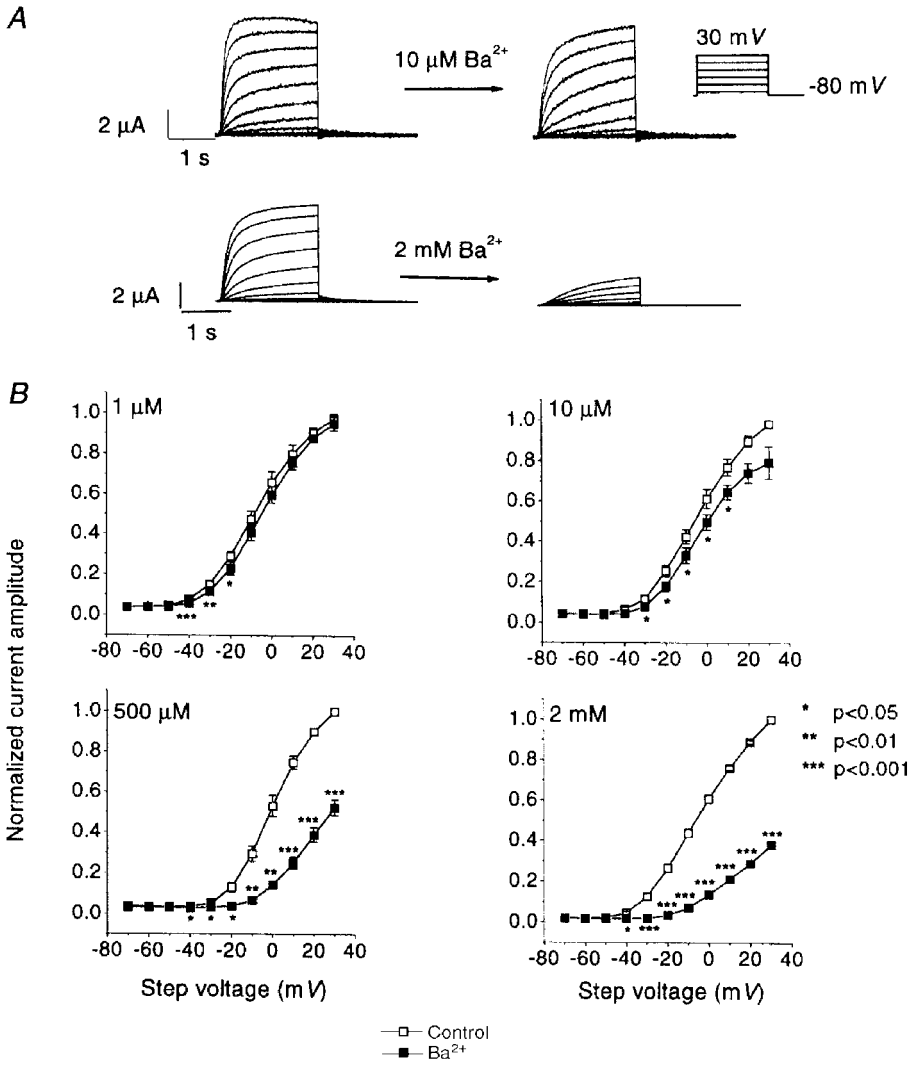

Figure 5. Response of the HERG S631A mutant to Ba^{2+}

A, I_{S631A} (left panels) recorded from two different oocytes during the application of pulse protocol (inset) identical to that used in Fig. 1. Effects of 10 μM and 2 mM Ba^{2+} on these currents are illustrated on the right. *B*, mean data for Ba^{2+} inhibition of step current carried by S631A mutant channels. Step current amplitudes were measured before and after 3 min of perfusion with the indicated Ba^{2+} concentrations, with the use of the voltage protocol illustrated above. Currents in each oocyte were normalized to the maximum current under control conditions, to control for varying current amplitudes among oocytes. The results shown are from 5, 5, 5 and 7 oocytes at 1, 10, 500 μM and 2 mM Ba^{2+}, respectively. Data are plotted as means ± S.E.M.; $*P < 0{\cdot}05$, $**P < 0{\cdot}01$, $***P < 0{\cdot}001$ *vs.* control.

Mathematical model of Ba^{2+} effects on I_{HERG}

In order to provide a quantitative explanation for the Ba^{2+}-dependent alterations in kinetics, half-activation voltage, and maximal conductance of HERG, we applied a mathematical model of the channel and its interaction with Ba^{2+}. Our model is based on the work of (Wang *et al.* 1997*a*), who developed a mathematical model of wild-type *HERG* channels expressed in *Xenopus* oocytes, based on two-electrode and cut-open oocyte clamp current recordings. They showed that the best fit to their data was obtained using a model with three closed states (C_2, C_1, C_0), one open state (O), and one inactivated state (I) (Scheme 1; Wang *et al.* 1997*a*).

Depolarization

$$C_2 \underset{\beta_{a0}}{\overset{\alpha_{a0}}{\rightleftharpoons}} C_1 \underset{k_b}{\overset{k_f}{\rightleftharpoons}} C_0 \underset{\beta_{a1}}{\overset{\alpha_{a1}}{\rightleftharpoons}} O \underset{\beta_i}{\overset{\alpha_i}{\rightleftharpoons}} I$$

Repolarization

Scheme 1

We implemented their formulation exactly, except for one modification to the inactivation kinetics of *HERG* that prevented the large initial current spikes observed at positive step potentials (+30 mV) in the original model. Faster inactivation kinetics reduced the amplitude of the spike, consistent with experimental recordings (Fig. 1).

The resulting modified functions for the rate constants of the O $\rightleftharpoons$ I transition are:

$$\alpha_i = 336{\cdot}6e^{0{\cdot}018412V}\ s^{-1}$$

and

$$\beta_i = 16{\cdot}7584e^{-0{\cdot}031588V}\ s^{-1}.$$

After establishing the basic model for wild-type I_{HERG}, we investigated the consequences of voltage-dependent or independent binding of Ba^{2+} to one or more channel states, aiming to reproduce the altered kinetics, half-activation voltage and maximal conductance of I_{HERG} in the presence of Ba^{2+}. The strong block immediately after depolarization and the more pronounced sigmoid activation profile of I_{HERG} in the presence of Ba^{2+} at negative potentials suggest closed state block. The absence of significant steady-state block at positive potentials suggests voltage-dependent action. Acceleration of tail current decay in the presence of Ba^{2+} requires shunting of open channels through open-blocked and closed-blocked states.

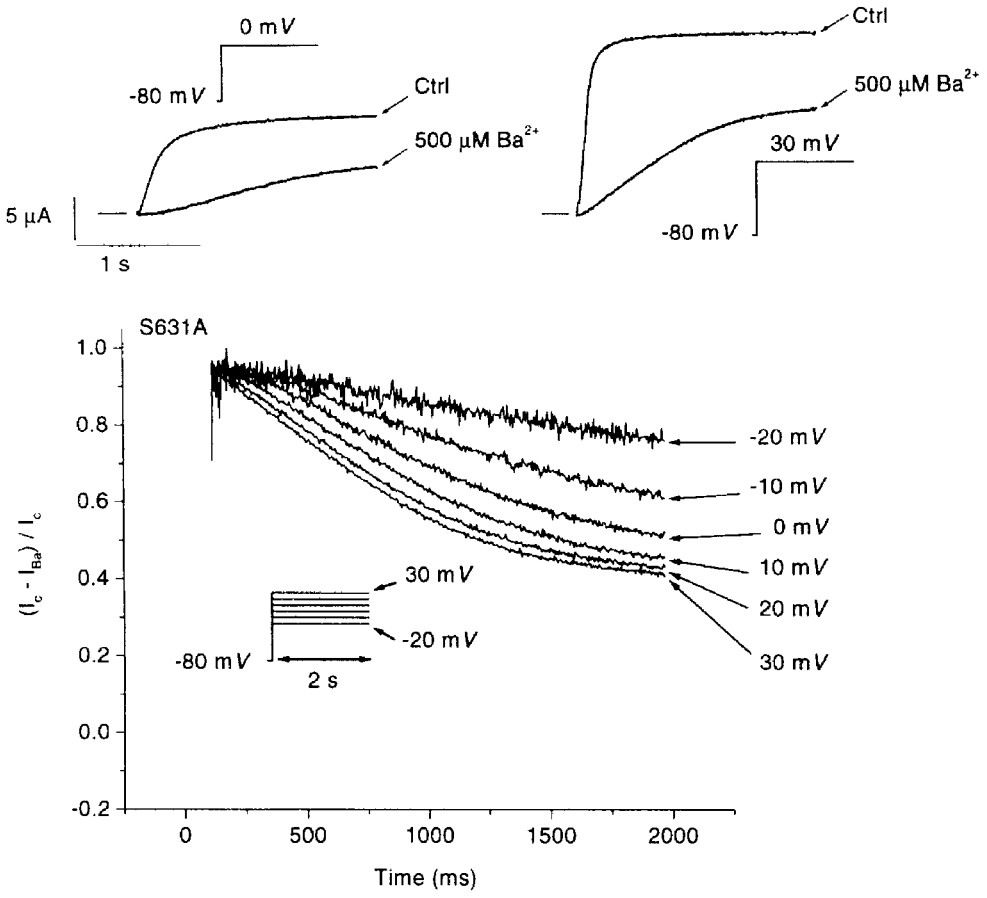

Figure 6. Evolution of Ba^{2+} block of current in S631A mutant channels during depolarizing steps

Top panel, original recordings during 2 s depolarizations to 0 mV (left) and 30 mV (right) before and after superfusion with 500 μM Ba^{2+}. Capacitive transients have been removed. Bottom, development of fractional block, $(I_c - I_{Ba})/I_c$, in the presence of 500 μM Ba^{2+} in the same experiment, upon depolarization to the 6 voltage levels indicated. Similar results were obtained in 6 other oocytes.

Based on the available data, we selected a simple model of voltage-dependent Ba^{2+} binding. This is in general terms similar to the Ba^{2+} blocking scheme suggested by Ho *et al.* (1999); however, these investigators did not study a full HERG model incorporating inactivation, which prevented them from drawing conclusions about the role of Ba^{2+} in decreasing maximal HERG tail currents and from fully understanding effects at voltages with substantial inactivation. We assumed that Ba^{2+} blocked only non-inactivated HERG channels, since we had no direct experimental evidence to suggest a role for binding of Ba^{2+} to the inactivated state. In addition, the low level of I_{HERG} block at positive potentials makes high affinity for inactivated channels unlikely. The $O \rightleftharpoons I$ transition was maintained in the model so as to simulate all the gating properties in the absence and presence of Ba^{2+}. Four new states are included in the model, C_0B, C_1B, C_2B and OB, corresponding to barium-bound closed and open states. Based on the step current values in the presence of Ba^{2+}, its binding affinity for the closed and open states is high at negative potentials and low at positive potentials. A unique steady-state relation for both the $C_{0,1,2} \rightleftharpoons C_{0,1,2}B$ and $O \rightleftharpoons OB$ transitions in the presence of Ba^{2+} at a 100 μM concentration was formulated as:

$$SS_{CCB,OOB} = (1 + e(V - 10)/15)^{-1}.$$

Rapid unblocking of step currents at +30 mV suggests rapid kinetics of Ba^{2+} interaction at positive potentials. Acceleration of tail currents suggests rapid blocking kinetics for high Ba^{2+} concentrations at negative potentials. The resulting fitted functions of the rate constants for the $C_{0,1,2} \rightleftharpoons C_{0,1,2}B$ and $O \rightleftharpoons OB$ transitions are:

$$\beta_{CCB,OOB} = 0{\cdot}78718e^{0{\cdot}065206V}\ s^{-1}$$

and

$$\alpha_{CCB,OOB} = [Ba^{2+}]0{\cdot}015332e^{-0{\cdot}001461V}\ s^{-1}.$$

The model parameters describing the transitions between states $C_{0,1,2}B$ and OB are identical to those describing the transitions between states $C_{0,1,2}$ and O, suggesting similar voltage-dependent effects on Ba^{2+} interaction with the closed and open states.

The voltage protocol used in Fig. 1*A* was applied to the model to produce model-generated step and tail currents in the

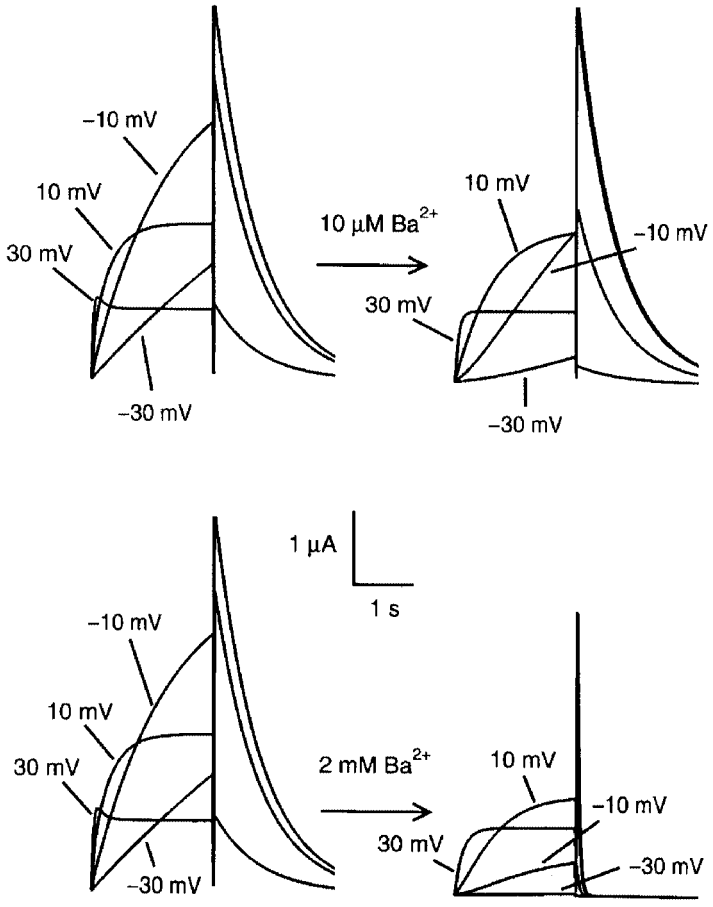

Figure 7. Model-simulated I_{HERG} in the absence and presence of low (10 μM) and high (2 mM) Ba^{2+} concentrations

Applied pulse protocols were identical to those used experimentally, i.e. −80 mV holding potential and 2 s depolarizations to the test voltages followed by return to the holding potential. Note the similarity in responses to experimental recordings (Fig. 1*A*).

presence of 10 μM and 2 mM Ba^{2+} (Fig. 7). An I_{HERG} reversal potential (V_{rev}) of −90 mV was used, and the maximum I_{HERG} conductance (g_{max}) was 0·72542 mS. Instantaneous I_{HERG} was then computed as $I_{HERG} = g_{max} O (V - V_{rev})$. The model reproduces the experimentally observed voltage-dependent step current block, delayed current activation and acceleration of tails caused by Ba^{2+} in a concentration-dependent manner (compare Fig. 7 with Fig. 1*A*). The quantitative results of the model simulations are summarized in the form of step (left) and tail (right) current–voltage relations at different Ba^{2+} concentrations in Fig. 8. The model accurately reproduces the main features of the corresponding experimental observations shown in Figs 2 and 3.

We then turned to the assessment of model predictions about Ba^{2+} interaction with the S631A mutant. The I_{HERG} model based on wild-type data could be modified to reproduce currents carried by S631A mutant channels simply by incorporating a +120 mV shift in inactivation voltage dependence (Fig. 9*A*). The shift required is close to the +102 mV experimentally measured shift reported by Zou *et al.* (1998). As was noted in experimental recordings (Fig. 5*A*), 2 mM Ba^{2+} substantially reduced step currents in the model at all voltages (Fig. 9*A*, right). The results of voltage steps were then analysed in the model for both drug-free I_{S631A} and I_{S631A} in the presence of various Ba^{2+} concentrations. Substantial concentration-dependent step current block by Ba^{2+} was observed at positive potentials (Fig. 9*B*), in contrast to the lack of block at positive potentials in the wild-type model (Fig. 8, left panels) and in agreement with the experimental results with the mutant (Fig. 5*B*). Figure 10 illustrates the evolution of Ba^{2+} block as a function of time during depolarizing voltage steps in the wild-type (upper panel) and the mutant (lower panel) model. The wild-type model reproduces the experimentally observed profiles (Fig. 4, bottom panel), with rapid unblocking at more positive potentials and slower, incomplete unblocking at lesser potentials. The model for the mutant (Fig. 10*B*) reproduces the reduced degree of Ba^{2+} unblocking observed for I_{S631A} (Fig. 6, bottom panel), although unblocking in the model remains faster than that observed experimentally.

DISCUSSION

We have demonstrated that Ba^{2+} inhibits I_{HERG} in a concentration-, voltage- and time-dependent fashion. An unusual aspect of Ba^{2+} block of I_{HERG} is its complete relief at positive voltages, which was no longer present in an inactivation-deficient mutant, suggesting that the phenomenon is related to rapid C-type inactivation. A mathematical model of HERG–Ba^{2+} interaction incorporating voltage-dependent Ba^{2+} block of open and closed states and no binding to the inactivated state provided simulations that were in broad agreement with experimental observations.

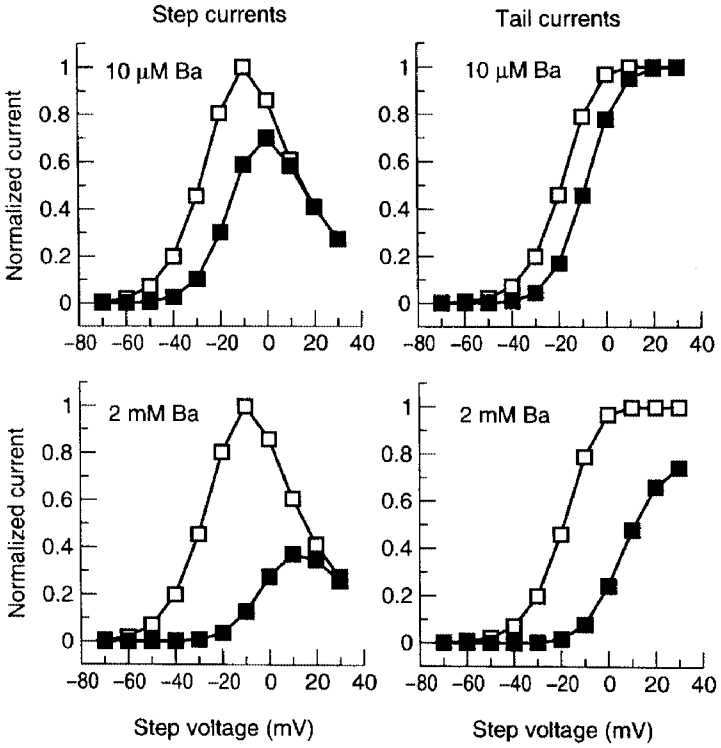

Figure 8. Current–voltage relations from model simulations of wild-type step and tail currents in the absence and presence of Ba^{2+}

The model was subjected to the pulse protocol studied in Fig. 7. Step current amplitudes (left panels) were calculated from simulated current at the end of 2 s depolarizing pulses. Tail currents (right panels) were obtained from current amplitudes upon returning to −80 mV.

Comparison with previous observations of Ba^{2+} block of I_{HERG}

Studies of Ba^{2+} interaction with I_{HERG} have been limited. Trudeau *et al.* (1995) showed that Ba^{2+} inhibits inward currents carried by I_{HERG}, with an ~50% reduction at 0·5 mM concentration. They did not observe time- or voltage-dependent block under a limited range of conditions. Subsequent to the completion and initial submission of the present study, Ho *et al.* (1999) reported a detailed analysis of the effects of divalent cations, including Ba^{2+}, on I_{HERG}. They noted a variety of effects of Ba^{2+} on I_{HERG} similar to those we observed, including voltage-dependent effects on step current, a slowing in the onset of step currents and an acceleration of tail currents. They were able to simulate effects on I_{HERG} activation voltage dependence and tail current kinetics on the basis of a voltage-dependent interaction of Ba^{2+} with open channels qualitatively similar to that incorporated in our model. Their model did not incorporate I_{HERG} inactivation and they only studied Ba^{2+} effects on currents carried by wild-type HERG channels.

Ho *et al.* (1999) justified the omission of channel inactivation in their model because the inactivation process seemed little affected by Ba^{2+}. Our observations also suggest little direct interaction between Ba^{2+} and I_{HERG} inactivation; however, inactivation appears to play a potentially important role in determining blocking behaviour at positive potentials, as shown by our results with the S631A mutant and supported by our modelling work. The loss of Ba^{2+} block of I_{HERG} step currents at positive potentials (Fig. 2) was no longer evident in the mutant (Fig. 5*B*), and the strong time-dependent unblocking during steps to positive potentials (Fig. 4, bottom) seen with wild-type channels was greatly attenuated in the mutant (Fig. 6, bottom). Furthermore, simply shifting inactivation by +120 mV in the mathematical model of HERG was sufficient to reproduce the major experimentally observed alterations in Ba^{2+} action caused by the S631A mutation. These results suggest that Ba^{2+} has negligible affinity for HERG channels in the inactivated state. Thus, at positive potentials there is a functional competition between Ba^{2+} block and the

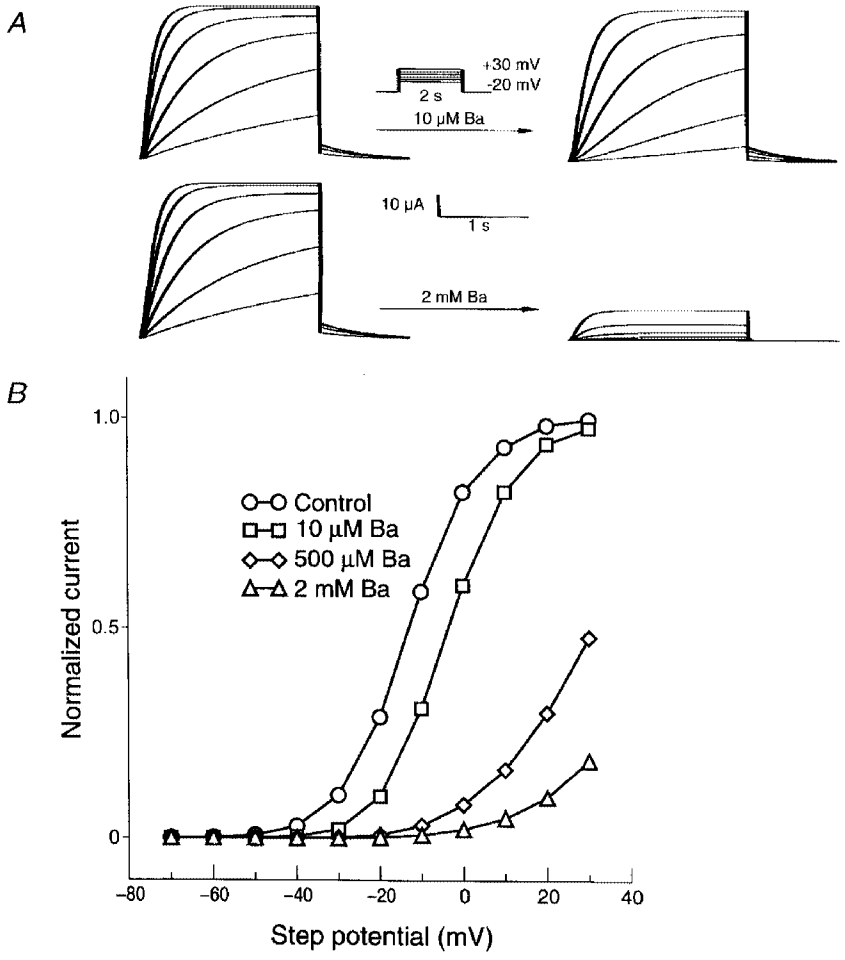

Figure 9. Model-simulated S631A currents in the absence and presence of low (10 µM) and high (2 mM) Ba^{2+} concentrations (*A*) and their representative current–voltage relationships under control conditions and in the presence of 10, 500 µM and 2 mM Ba^{2+} (*B*)

Note the similarity of the simulated current profiles to experimental results (Fig. 5).

inactivation process for removal of channels from the open state. At such potentials, the steady-state ratio of inactivated to open channels is much greater than that between Ba^{2+} blocked and unblocked open channels, resulting in negligible effects of Ba^{2+} on the number of conducting, open channels. In the mutant, inactivation is greatly attenuated or lost over the voltage range examined in the present study, and the blocking of open channels is apparent at positive voltages.

Comparison with Ba^{2+} effects on other K^+ channels

Ba^{2+} has long been known to interact with a variety of native K^+ channels (Werman & Grundfest, 1961). Eaton & Brodwick (1980) showed that Ba^{2+} inhibits K^+ currents in squid giant axon upon either external or internal application. Ba^{2+} block is voltage and time dependent, with features that suggest a blocking site in the middle of the membrane electrical field. Increasing external [K^+] decreases block by external Ba^{2+}, suggesting that Ba^{2+} and K^+ compete for a common binding site. Armstrong *et al.* (1982) further evaluated Ba^{2+} interactions with the squid K^+ conductance, noting that internal Ba^{2+} enters the channel only when activation gates are open, producing time-dependent block and that the entry of external Ba^{2+} is particularly remarkable when the activation gates are closed. The blocking site appears to be the same for both external and internal Ba^{2+}, and is located towards the internal mouth of the channel, two thirds of the way from the external side. Ba^{2+} is a strong blocker of inward rectifier cardiac K^+ channels, blocking both the background conductance (I_{K1}) and the acetylcholine-activated conductance (I_{KACh}) with 50%-inhibitory concentrations in the range of 10 to 20 μM (Carmeliet & Mubagwa, 1986). Ba^{2+} block of I_{KACh} is subject to the same type of 'knock-off' interaction with external K^+ as seen for the K^+ conductance in squid giant axon, and shows time dependence.

Over the past several years, substantial work has been performed to evaluate the interaction between Ba^{2+} and various cloned K^+ channels, primarily to assess structural determinants of Ba^{2+} block. Hurst *et al.* (1995) showed that exposure of *Shaker* channels in *Xenopus* oocytes to external Ba^{2+} is followed by progressive channel block with two kinetic phases, apparently due to distinct blocking sites. The rapid-component site has relatively low affinity (K_d at 0 mV of about 19·1 mM) and its Ba^{2+} affinity is less voltage dependent than the slower site. The same group subsequently showed that mutations in the pore region of *Shaker* could reduce Ba^{2+} block by decreasing the rate of block (Hurst *et al.* 1996). Harris *et al.* (1998) studied the properties of Ba^{2+} block of *Shaker* further and identified three potential interaction sites. All three sites are accessible to the external solution when the activation gates are closed, and the deep site lies between the activation gate and the structure responsible for C-type inactivation. They also identified mutations in the pore region that disrupt two of the binding sites. More recently Basso *et al.* (1998) determined that Ba^{2+} binds tightly to C-type inactivated *Shaker* channels, with C-type inactivation creating high-energy barriers that hinder Ba^{2+} egress. Ba^{2+} also interacts with Kv2.1 channels, with block occurring at both internal and external sites, and showing strong voltage and state dependence (Taglialatela *et al.* 1993).

Some of the properties of Ba^{2+} block of I_{HERG} resemble those previously reported for other K^+ channels as discussed above. These include the voltage dependence of block, with inhibition more marked at negative voltages, and the time dependence of blocking behaviour. The feature which appears to differentiate Ba^{2+} block of I_{HERG} and that of

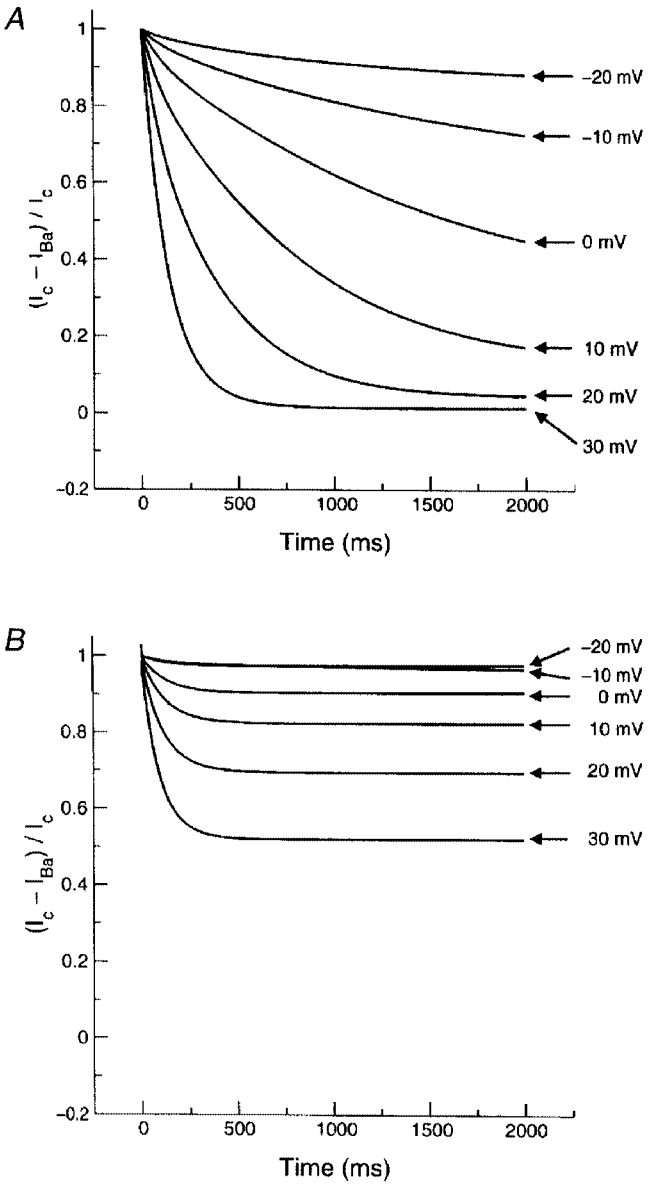

Figure 10. Model-simulated fractional Ba^{2+} block of wild-type (top panel) and S631A mutant (lower panel) currents during 2 s voltage steps

Note the prominent unblocking of Ba^{2+} from wild-type channels at positive potentials, similar to experimental observations (Fig. 4, lower panel). Note also the attenuation of unblocking in the simulations for the mutant (compare with experimental observations in Fig. 6, lower panel).

other channels studied to date (which have generally lacked inactivation) is the strong attenuation of I_{HERG} block at positive potentials related to the presence of an intact rapid C-type inactivation mechanism.

Potential limitations

It would have been desirable to isolate Ba^{2+} block of individual channel states with selective voltage protocols, in order to test state-dependent block of the model both directly and independently. Unfortunately, because Ba^{2+} interacts with closed and open channel states, it is impossible to design voltage protocols that evaluate Ba^{2+} block of single states. For example, for HERG channels in the absence of Ba^{2+}, the inactivated state can be studied by pulsing briefly from a positive (e.g. 30 mV) to a negative voltage (e.g. −120 mV) to remove inactivation and then observing fast inactivation during a pulse to a positive potential. However, Ba^{2+} blocks closed channels in a time-dependent way on pulsing to the negative potential and will unblock in a time-dependent way on pulsing back to the more positive potential. Thus, the peak current during the final depolarizing pulse will reflect both intrinsic voltage-dependent conductance and Ba^{2+} block of open and closed channels. The kinetics of current decay will reflect intrinsic inactivation, but also the kinetic changes in Ba^{2+} block as channels cycle through closed, open and inactivated states. The closed state cannot be studied in isolation because channels have to be opened to record current and evaluate block. The open state cannot be studied in isolation because some degree of inactivation occurs in wild-type channels over most of the voltage range over which there is significant channel opening. Therefore, we relied on the use of an inactivation-deficient mutant and mathematical modelling to understand the Ba^{2+} interaction with the channel.

At some test potentials (particularly negative to 0 mV), steady-state current was not achieved at the end of a 2 s voltage pulse. This could have affected the derived half-activation voltages. In addition, a direct effect of Ba^{2+} to slow activation could have contributed to apparent unblocking by reducing current at the beginning of a pulse. A slowing in activation cannot be clearly separated experimentally from time-dependent unblocking of inactivated channels. The more marked slowing of current development during a pulse in wild-type (e.g. Fig. 1, −10 mV) compared with inactivation-deficient (Fig. 5, top) channels argues in favour of unblocking during inactivation as an important mechanism for apparent slowing of wild-type activation in the presence of Ba^{2+}. Nonetheless, a possible contribution from Ba^{2+}-induced activation slowing cannot be excluded.

Divalent cations can cause voltage shifts of activation and inactivation, which can complicate analysis of their direct actions. In a separate set of experiments, we applied a three-step protocol to examine the voltage dependence of inactivation in oocytes expressing *HERG*. Only a modest shift (~10 mV) of the voltage dependence was observed with 500 μM or 2 mM Ba^{2+} (data not shown), in agreement with the observations of Ho *et al.* (1999). This moderate shift would not explain phenomenon at very positive voltages, at which inactivation is saturated. We also studied the effects of Ba^{2+} in neuraminidase-treated oocytes. Neuraminidase is known to selectively hydrolyse negatively charged sialic acid groups on the cell surface, eliminating their potential influence on voltage-dependent gating processes (Fermini & Nathan, 1991). Effects of neither 500 μM nor 2 mM Ba^{2+} ($n = 5$ each) were quantitatively different in neuraminidase treated *vs.* untreated oocytes (data not shown). Nonetheless, we cannot exclude a possible contribution of surface charge screening effects to the voltage-dependent actions of Ba^{2+}, nor can we be positive that the S631A mutant had no effect on affinity for Ba^{2+} independent of effects on C-type inactivation.

Although our mathematical model reproduced many of the features of currents carried by wild-type and S631A HERG in the absence and presence of Ba^{2+}, not all experimental findings were noted in the model. Most notably, the rate of apparent Ba^{2+} unblocking during step pulses in mutant channels was slower in experimental recordings (Fig. 6) than predicted by the model (Fig. 10*B*). Some of the discrepancies may be due to our use of the model of Wang *et al.* (1997*a*) with minimal modification. However, it is quite possible that our relatively simple model does not take into consideration additional complexities of the Ba^{2+}–HERG interaction. In addition, the agreement between model predictions and experimental behaviour does not prove the validity of the assumptions underlying the model. It simply indicates that the conceptual notions incorporated in the model are sufficient to explain most of the observed behaviour. We cannot eliminate the possibility that an alternative model based on a different set of assumptions could account for experimental behaviour just as well.

Novel aspects and potential importance

The *HERG* gene sprang into popular attention upon the demonstration of the role of *HERG* mutations in the type 2 congenital long QT syndrome (Curran *et al.* 1995). HERG was found to encode a channel with macroscopic current properties corresponding to I_{Kr} (Sanguinetti *et al.* 1995; Trudeau *et al.* 1995). The single-channel properties of I_{HERG} and its pharmacologic responses were also found to resemble those of I_{Kr} (Kiehn *et al.* 1996; Zou *et al.* 1997). One of the distinctive properties of I_{Kr} is its strong inward rectification, caused by very rapid C-type inactivation of the HERG channel (Smith *et al.* 1996; Spector *et al.* 1996). This unusual form of inactivation is probably central to the physiological role of the channel, allowing it to contribute importantly to phase 3 repolarization without interfering with the long plateau phase which is typical of cardiac action potentials and essential to normal mechanical and electrical function. Rapid C-type inactivation is associated with the specific pharmacological sensitivity of I_{Kr} to methanesulfonanilides like dofetilide, and mutations that remove fast inactivation (like the S631A mutation which we

studied) greatly reduce sensitivity to methanesulfonanilide block (Wang *et al.* 1997*b*; Ficker *et al.* 1998). We found that the C-type inactivation mechanism of I_{HERG} was associated with unusual behaviour of Ba^{2+} block, with strong unblocking of wild-type channels at positive voltages that disappeared when fast inactivation was removed. It is perhaps because of this behaviour that Ba^{2+} block of I_{Kr} has not previously been noted – the rapid inactivation mechanism of the channel minimizes block by Ba^{2+} at voltages positive to 0 mV. It is presently unknown, and would be interesting to determine, whether Ba^{2+} unblocking in the presence of inactivation is limited to I_{HERG}, or also occurs with other K^+ channels demonstrating inactivation. A variety of other divalent cations, including Mn^{2+}, Zn^{2+}, Ca^{2+} and Mg^{2+}, also show reduced ability to block I_{HERG} at positive potentials (Ho *et al.* 1998, 1999). It would be interesting to establish whether the removal of inactivation alters their interactions with I_{HERG}, and to determine the molecular mechanism of this phenomenon. Futhermore, it would be interesting to determine how co-expression with *MiRP* alters *HERG* block by Ba^{2+} and other cations, since native I_{Kr} is believed to be carried by channel complexes involving both *HERG* and *MiRP* (Abbott *et al.* 1999).

Ba^{2+} has been used extensively to eliminate potential contaminating effects of I_{K1} channels in the recording of other K^+ currents (DiFrancesco *et al.* 1984; Shimoni *et al.* 1992; Brochu *et al.* 1992; Li *et al.* 1996). Based on similar reasoning with respect to the specificity of Ba^{2+} for I_{K1} inhibition, Ba^{2+} has also been used to examine the potential role of I_{K1} as a repolarizing current in intact heart studies (Gillis *et al.* 1998). Paquette *et al.* (1998) studied the effects of a variety of divalent cations on I_{Kr} in rabbit ventricular myocytes, but time-dependent I_{K1} block precluded evaluation of the effects of Ba^{2+} on I_{Kr}. Since I_{K1} is time dependent at some voltages and Ba^{2+} block is itself time and voltage dependent, studies of Ba^{2+} effects on I_{Kr} in native myocytes are difficult to perform and interpret. Nonetheless, our observations urge caution in the use of Ba^{2+} as a tool to remove or isolate effects on I_{K1}, since I_{HERG} (and presumably the native equivalent I_{Kr}) can be suppressed by relatively low Ba^{2+} concentrations.

Abbott, G. W., Sesti, F. S., Splawski, I., Buck, M. E., Lehmann, M. H., Timothy, K. W., Keating, M. T. & Goldstein, S. A. (1999). MiRP1 forms I_{Kr} potassium channels with HERG and is associated with cardiac arrhythmia. *Cell* **97**, 175–187.

Anumonwo, J. M. B., Freeman, L. C., Kwok, W. M. & Kass, R. S. (1992). Delayed rectification in single cells isolated from guinea pig sinoatrial node. *American Journal of Physiology* **262**, H921–925.

Armstrong, C. M., Swenson, R. P. & Taylor, S. R. (1982). Block of squid axon K channels by internally and externally applied barium ions. *Journal of General Physiology* **80**, 663–682.

Balser, J. R., Bennett, P. B. & Roden, D. M. (1990). Time-dependent outward current in guinea pig ventricular myocytes, gating kinetics of the delayed rectifier. *Journal of General Physiology* **96**, 835–863.

Barhanin, J., Lesage, F., Guillemare, E., Fink, M., Lazdunski, M. & Romey, G. (1996). K (V)LQT1 and lsK (minK) proteins associate to form the I(Ks) cardiac potassium current. *Nature* **384**, 78–80.

Barry, D. M. & Nerbonne, J. M. (1996). Myocardial potassium channels: electrophysiological and molecular diversity. *Annual Review of Physiology* **58**, 363–394.

Basso, C., Labarca, P., Stefani, E., Alvarez, O. & Latorre, R. (1998). Pore accessibility during C-type inactivation in Shaker K^+ channels. *FEBS Letters* **429**, 375–380.

Berthet, M., Denjoy, I., Donger, C., Demay, L., Hammoude, H., Klug, D., Schulze-Bahr, E., Richard, P., Funke, H., Schwartz, K., Coumel, P., Hainque, B. & Guicheney, P. (1999). C-terminal HERG mutations: the role of hypokalemia and a KCNQ1-associated mutation in cardiac event occurrence. *Circulation* **99**, 1464–1470.

Brochu, R. M., Clay, J. R. & Shrier, A. (1992). Pacemaker current in single cells and in aggregates of cells dissociated from the embryonic chick heart. *Journal of Physiology* **454**, 503–515.

Carmeliet, E. & Mubagwa, K. (1986). Characterization of the acetylcholine-induced potassium current in rabbit cardiac Purkinje fibres. *Journal of Physiology* **371**, 219–237.

Colatsky, T. J., Follmer, C. H. & Starmer, C. F. (1990). Channel specificity in antiarrhythmic drug action. Mechanism of potassium channel block and its role in suppressing and aggravating cardiac arrhythmias. *Circulation* **82**, 2235–2242.

Curran, M. E., Splawski, I., Timothy, K. W., Vincent, G. M., Green, E. D. & Keating, M. T. (1995). A molecular basis for cardiac arrhythmia: HERG mutations cause long QT syndrome. *Cell* **80**, 795–803.

DiFrancesco, D., Ferroni, A. & Visentin, S. (1984). Barium-induced blockade of the inward rectifier in calf Purkinje fibres. *Pflügers Archiv* **402**, 446–453.

Eaton, D. C. & Brodwick, M. S. (1980). Effects of barium on the potassium conductance of squid axon. *Journal of General Physiology* **75**, 727–750.

Fermini, B. & Nathan, R. D. (1991). Removal of sialic acid alters both T- and L-type calcium currents in cardiac myocytes. *American Journal of Physiology* **260**, H735–743.

Ficker, E., Jaroliemek, W., Kiehn, J., Baumann, A. & Brown, A. M. (1998). Molecular determinants of dofetilide block of HERG K^+ channels. *Circulation Research* **82**, 386–395.

Giles, W. R. & Shibata, E. F. (1985). Voltage clamp of bull-frog cardiac pace-maker cells: a quantitative analysis of potassium currents. *Journal of Physiology* **368**, 265–292.

Gillis, A. M., Geonzon, R. A., Mathison, H. J., Kulisz, E., Lester, W. M. & Duff, H. J. (1998). The effects of barium, dofetilide and 4-aminopyridine (4-AP) on ventricular repolarization in normal and hypertrophied rabbit heart. *Journal of Pharmacology and Experimental Therapeutics* **285**, 262–270.

Harris, R. E., Larsson, H. P. & Isacoff, E. Y. (1998). A permeant ion binding site located between two gates of the *Shaker* K^+ channel. *Biophysical Journal* **74**, 1808–1820.

Hebert, T. E., Monette, R., Drapeau, P. & Dunn, R. J. (1994). Voltage dependencies of the fast and slow gating modes of RIIA sodium channels. *Proceedings of the Royal Society* B **256**, 253–261.

Hille, B. (1992). *Ionic Channels of Excitable Membranes*. Sinauer Associates Inc. Publishers, Sunderland, MA, USA.

Ho, W.-K., Kim, I., Lee, C. O. & Earm, Y. E. (1998). Voltage-dependent blockade of HERG channels expressed in *Xenopus* oocytes by external Ca^{2+} and Mg^{2+}. *Journal of Physiology* **507**, 631–638.

Ho, W.-K., Kim, I., Lee, C. O., Youm, J. B., Lee, S. H. & Earm, Y. E. (1999). Blockade of HERG expresssed in *Xenopus laevis* oocytes by external divalent cations. *Biophysical Journal* **76**, 1959–1971.

Hurst, R. S., Latorre, R., Toro, L. & Stefani, E. (1995). External barium block of *Shaker* potassium channels: evidence for two binding sites. *Journal of General Physiology* **106**, 1069–1087.

Hurst, R. S., Toro, L. & Stefani, E. (1996). Molecular determinants of external barium block in *Shaker* potassium channels. *FEBS Letters* **388**, 59–65.

Kiehn, J., Lacerda, A. E., Wible, B. & Brown, A. M. (1996). Molecular physiology and pharmacology of HERG. Single-channel currents and block by dofetilide. *Circulation* **94**, 2572–2579.

Li, G. R., Feng, J., Yue, L., Carrier, M. & Nattel, S. (1996). Evidence for two components of delayed rectifier K^+ current in human ventricular myocytes. *Circulation Research* **78**, 689–696.

Miller, C., Latorre, R. & Reisin, I. (1987). Coupling of voltage-dependent gating and Ba^{2+} block in the high-conductance, Ca^{2+}-activated K^+ channel. *Journal of General Physiology* **90**, 427–449.

Noble, D. & Tsien, R. W. (1969). Outward membrane currents activated in the plateau range of potentials in cardiac Purkinje fibres. *Journal of Physiology* **200**, 205–231.

Paquette, T., Clay, J. R., Ogbaghebriel, A. & Shrier, A. (1998). Effects of divalent cations on the E-4031-sensitive repolarization current, I_{Kr}, in rabbit ventricular myocytes. *Biophysical Journal* **74**, 1278–1285.

Sanguinetti, M. C., Curran, M. E., Zou, A., Shen, J., Spector, P. S., Atkinson, D. L. & Keating, M. T. (1996). Coassembly of K(V)LQT1 and minK (IsK) proteins to form cardiac I(Ks) potassium channel. *Nature* **384**, 80–83.

Sanguinetti, M. C., Jiang, C., Curran, M. E. & Keating, M. T. (1995). A mechanistic link between an inherited and an acquired cardiac arrhythmia: HERG encodes the I_{Kr} potassium channel. *Cell* **81**, 1–20.

Sanguinetti, M. C. & Jurkiewicz, N. K. (1990). Two components of cardiac delayed rectifier K^+ current. Differential sensitivity to block by class III antiarrhythmic agents. *Journal of General Physiology* **96**, 195–215.

Sanguinetti, M. C. & Jurkiewicz, N. K. (1991). Delayed rectifier outward K^+ current is composed of two currents in guinea pig atrial cells. *American Journal of Physiology* **260**, H393–399.

Shimoni, Y., Clark, R. B. & Giles, W. R. (1992). Role of an inwardly rectifying potassium current in rabbit ventricular action potential. *Journal of Physiology* **448**, 709–727.

Smith, P. L., Baukrowitz, T. & Yellen, G. (1996). The inward rectification mechanism of the HERG cardiac potassium channel. *Nature* **379**, 833–836.

Spector, P. S., Curran, M. E., Zou, A., Keating, M. T. & Sanguinetti, M. C. (1996). Fast inactivation causes rectification of the I_{Kr} channel. *Journal of General Physiology* **107**, 611–619.

Taglialatela, M., Drewe, J. A. & Brown, A. M. (1993). Barium blockade of a clonal potassium channel and its regulation by a critical pore residue. *Molecular Pharmacology* **44**, 180–190.

Trudeau, M. C., Warmke, J. W., Ganetzky, B. & Robertson, G. A. (1995). HERG, a human inward rectifier in the voltage-gated potassium channel family. *Science* **269**, 92–95.

Wang, Q., Curran, M. E., Splawski, I., Burn, T. C., Millholland, J. M., VanRaay, T. J., Shen, J., Timothy, K. W., Vincent, G. M., de Jager, T., Schwartz, P. J., Toubin, J. A., Moss, A. J., Atkinson, D. L., Landes, G. M., Connors, T. D. & Keating, M. T. (1996). Positional cloning of a novel potassium channel gene: KVLQT1 mutations cause cardiac arrhythmias. *Nature Genetics* **12**, 17–23.

Wang, S., Liu, S., Morales, M. J., Strauss, H. C. & Rasmusson, R. L. (1997*a*). A quantitative analysis of the activation and inactivation kinetics of HERG expressed in *Xenopus* oocytes. *Journal of Physiology* **502**, 45–60.

Wang, S., Morales, M. J., Liu, S., Strauss, H. C. & Rasmusson, R. L. (1997*b*). Modulation of HERG affinity for E-4031 by $[K^+]_o$ and C-type inactivation. *FEBS Letters* **417**, 43–47.

Weerapura, M., Hebert, T. & Nattel, S. (1998). State-dependent barium block of HERG channels: mutual antagonism with inactivation. *Circulation* **98**, suppl I, I-126.

Werman, R. & Grundfest, H. (1961). Graded all-or-none electrogenesis in arthropod muscle. II. The effects of alkalai earth and onium ions on lobster muscle fibers. *Journal of General Physiology* **44**, 997–1027.

Zang, W. J., Yu, X. J. & Boyett, M. R. (1995). Barium block of the muscarinic potassium current in guinea-pig atrial cells. *Pflügers Archiv* **430**, 348–357.

Zou, A., Curran, M. E., Keating, M. T. & Sanguinetti, M. C. (1997). Single HERG delayed rectifier K^+ channels expressed in *Xenopus* oocytes. *American Journal of Physiology* **272**, H1309–1314.

Zou, A., Xu, Q. P. & Sanguinetti, M. C. (1998). A mutation in the pore region of HERG K^+ channels reduces rectification by shifting the voltage dependence of inactivation. *Journal of Physiology* **509**, 129–137.

Acknowledgements

HERG cDNA was a generous gift of Dr M. Keating and Dr M. Sanguinetti, University of Utah. The authors thank Luce Bégin for expert secretarial help. This work was supported by the Medical Research Council of Canada, the Quebec Heart Foundation, the Natural Science and Engineering Research Council and the Fonds de Recherche de l'Institut de Cardiologie de Montréal. T.E.H. and M.C. are research scholars of the Fonds de la Recherche en Santé du Québec, and M.W. is supported by a Medical Research Council studentship.

Corresponding author

S. Nattel: Research Center, Montreal Heart Institute, 5000 Bélanger Street East, Montreal, Quebec, Canada H1T 1C8.

Email: nattel@icm.umontreal.ca